

LABORATOIRE MATHÉMATIQUES APPLIQUÉES AUX SYSTÈMES

*Analysis of Diffusion Tensor Images from the
Human Skeletal Muscles*

Christian Wachinger — Lilla Zollei — Nikos Paragios — Jean-François Deux —
Guillaume Bassez — Alain Rahmouni

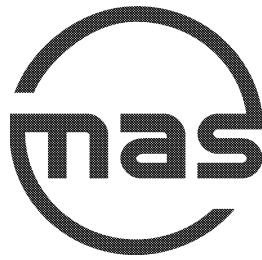
N° 0602

June 2006

Projet Orasis

RAPPORT DE RECHERCHE





Analysis of Diffusion Tensor Images from the Human Skeletal Muscles

Christian Wachinger ^{* †}, Lilla Zollei [‡], Nikos Paragios [‡], Jean-François Deux [§], Guillaume Bassez [§], Alain Rahmouni [§]

Projet Orasis — Imagerie Médicale et Vision par Ordinateur

Rapport de recherche n° 0602 — June 2006 — 33 pages

Abstract: The possibility of diffusion tensor imaging to discover anatomical muscular properties and the evolution of muscular diseases, especially Myopathy, was investigated. Statistical analysis was done on the tensor and fiber space. A change in the FA distribution between healthy and non-healthy tissue was discovered. Fiber clustering was applied with the expectation to reduce the number of fibers, to class fibers in muscle groups, and to distinguish between healthy and non-healthy fibers.

Key-words: DTI, Diffusion Tensor, Fiber, Tractography, Clustering, Human Skeletal Muscle, Calf

* Technical University of Munich

† Ecole Nationale Supérieure des Télécommunications Paris

‡ Ecole Centrale Paris

§ CHU-Henry Mondor Hospital, Créteil, Paris

Analyse des images diffusion

Résumé : The possibility of diffusion tensor imaging to discover anatomical muscular properties and the evolution of muscular diseases, especially Myopathy, was investigated. Statistical analysis was done on the tensor and fiber space. A change in the FA distribution between healthy and non-healthy tissue was discovered. Fiber clustering was applied with the expectation to reduce the number of fibers, to class fibers in muscle groups, and to distinguish between healthy and non-healthy fibers.

Mots-clés : DTI, Diffusion Tensor, Fiber, Tractography, Clustering, Human Skeletal Muscle, Calf

Contents

1	Introduction	5
1.1	Muscle architecture and Myopathy	6
2	Diffusion Tensor Imaging	7
2.1	Image Acquisition	7
2.2	Diffusion Measuring	8
2.3	Calculation of Diffusion Tensors	10
2.4	Interpretation of Diffusion Tensors	11
2.4.1	Eigenvalues and Eigenvectors	11
2.4.2	Anisotropy Indices	11
3	Pre-processing of images	12
3.1	Segmentation of muscles	12
3.1.1	Segmentation on anatomy images	13
3.1.2	Segmentation in tensor space	13
3.1.3	Segmentation in fiber space	14
3.1.4	Semi-automatic segmentation method	14
3.2	Registration	14
3.2.1	Intra subject	14
3.2.2	Inter subject	14
4	Fiber Tracking	15
4.1	Tracking algorithms	18
4.2	Algorithms in detail	18
4.3	Tractography results	19
5	Fiber Clustering	19
5.1	K-Means clustering	21
5.2	Joint probabilistic curve clustering and alignment	21

6	Results of Analysis	23
6.1	Muscle groups	23
6.1.1	Tensor space	23
6.1.2	Fiber space	24
6.2	Healthy and non-healthy muscle	26
6.2.1	Tensor space	26
6.2.2	Fiber space	27
7	Conclusions	27

1 Introduction

Myopathy is one of the most frequent skeletal muscular diseases, which leads to a reduction of the muscular performance. The performance and mechanical behavior of a muscle is determined by its architecture. The exact influence of the disease on the muscle architecture is not yet clear because there is a lack of 3D imaging modalities that are able to visualize the architecture. With the introduction of diffusion tensor imaging (DTI) [1] an imaging modality became available that enables to investigate the muscle microstructure and offers therefore an excellent opportunity to study the evolution of muscular diseases. Various methods that can be used for the investigation and obtained results are presented in this report.

Most DTI studies of the skeletal muscle focus on animals because the images can be taken with a higher resolution. The results of studies from the tibialis anterior muscle of a rat [2] and from the semimembranosus muscle of a cat [3] are that DTI fiber orientation coincides with skeletal muscle fiber direction. Damon et al. validated the usage of fiber tracking for in-vivo structural analysis of small-animal skeletal muscle. The ability of fiber tracking, to measure the fiber orientation (pennation) in skeletal muscle in-vivo, was quantitatively assessed. Heemskerk et al. showed the feasibility of diffusion tensor acquisition and fiber tracking for the skeletal muscle of mice, and thus the possibility to determine quantitatively the muscle architecture [4].

Only Galban et al. investigated the diffusion properties in humans, focusing on the human calf where seven muscle groups were segmented. Differences in diffusive parameter values occurred primarily between functionally different muscles. Also a strong correlation between the physiological cross-sectional area (PCSA) and the third eigenvalue of tensors was found. Leading to the hypothesis that the third eigenvalue depends on the radius of the fibers [5]. In a following study Galban et al. focused on the analysis of gender differences in the human skeletal muscle [6]. The results of the study show that water diffusion differs between males and females.

Muscular diseases are, so far, mostly investigated by biopsy with successive microscopy. This has several disadvantages. First, only a local analysis can be carried out. Second, it does not allow to take a series of measurements at different times. Third, full three-dimensional reconstruction is time consuming. Fourth, it does not allow to make in-vivo measurements. Using DTI eliminates these drawbacks and provides the opportunity to make global three-dimensional in-vivo studies over time of muscular diseases.

It is not yet clear to which extent DTI can be used to investigate muscular diseases, so that we try to get a better understanding of the possibilities of this imaging modality for the human calf. This is done in close cooperation with the CHU-Henry Mondor hospital (Creteil, Paris). The main interests lie in the characterization of muscular properties and effects of myopathies. It is of interest to quantify the amount of intact muscle tissue that remains in a calf affected by the disease and to give more accurate prognoses of the evolution of the disease.

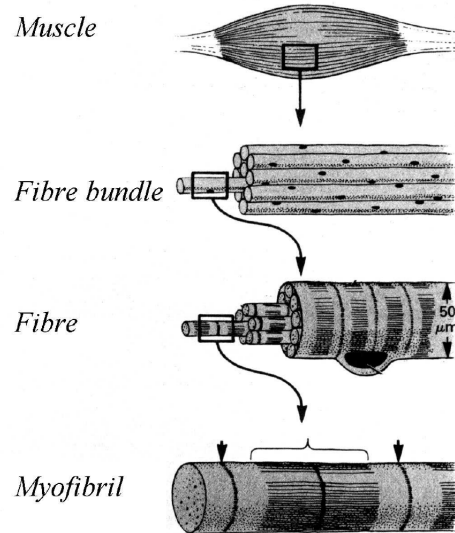


Figure 1: The structure of a muscle: muscle, fiber bundle, fiber and myofibril [8].

1.1 Muscle architecture and Myopathy

Muscle architecture is characterized by various parameters like the physiological cross-sectional area (PCSA), fiber length, and pennation angle. The pennation angle is the angle between the muscle fibers and the tendon plate. The PCSA is the sum of the cross-sectional areas of all fibers and the architectural parameter that is directly proportional to the maximum force generated by the muscle. The PCSA is the parameter the most difficult to measure and is therefore normally indirectly determined from the muscle volume and fiber length [7]. During our experiments we tried to determine these parameters for 7 different groups of muscles: soleus (SOL), lateral gastrocnemius (LG), medial gastrocnemius (MG), posterior tibialis (PT), anterior tibialis (AT), extensor digitorum longus (EDL), and peroneus longus (PL). The pennation angles are 50° , 50° , 15° , 15° , 32° , 5° , and 10° , respectively. And the fiber lengths are 2.6 cm, 2.5 cm, 2.4 cm, 5.6 cm, 2.8 cm, 9.4 cm, and 4.4 cm, respectively [5].

The myopathy is a neuromuscular disease that leads to muscular weakness. Muscular cells in the muscle are replaced by fat cells. The fat cells keep the regular fiber structure that was set up by the muscle cells, see Figure 1. Therefore, we assume that the disease does not lead to a change in the structure of the reconstructed fibers. But we assume that the disease leads to a change in the water diffusivity in the fibers, resulting in changing trace, FA, and ADC values along the fiber. These values are frequently used as stopping criteria for the fiber tracking algorithm so that less and smaller fibers should be found in the regions affected by the disease.

2 Diffusion Tensor Imaging

Diffusion Tensor Imaging measures the motion distribution of hydrogen atoms within water molecules. Water seems to be calm to the naked eye, but individual water molecules are constantly in motion and colliding with each other and other molecules in tissues at high speed. The effect of these collisions is that water molecules spread out or diffuse. This phenomenon is known as "Brownian motion". A concrete example illustrating the effect of diffusion is the spreading of ink in a glass of water.

In the example with the ink the diffusion is isotropic. But in the human body the diffusion is restricted by various tissues like organs, membranes and cell walls what leads to anisotropic diffusion. When averaging the diffusion over the macroscopic scale of an image voxel, the restriction is identical in all directions, so isotropic diffusion is measured. However, in tissues having a regularly ordered microstructure like cerebral white matter and muscle, the cellular arrangement shows a preferred direction of water diffusion that is largely uniform across the entire voxel, therefore anisotropic diffusion is measured. In the brain, for instance, the main direction of the water diffusion is along the longitudinal direction of the axons. The reason for the anisotropy of the diffusion are tightly packed multiple myelin membranes encompassing the axons and therefore limiting the motion of tissue water [9]. An effect similar to that can also be found in the muscles [5], with its highly ordered elongated muscle fibers, see Figure 1.

2.1 Image Acquisition

The acquisition of images showing in-vivo muscle diffusion anisotropy is quite recent, because there have been problems with the too weak gradients and the motion sensitivity. Just the introduction of diffusion-weighted echo-planar imaging (EPI) sequences, that replaced the conventional spin-echo sequences, decreased the sensitivity to motion artifacts [10]. Further advantages promises the tetrahedral gradient pattern that consists of four different combinations of x, y, and z gradients applied simultaneously at full strength to uniformly measure diffusion in four different directions [11]. The benefits are a better signal-to-noise ratio (SNR) than in the normal orthogonal case and the fact that it is readily implemented on clinical scanners [12]. Moreover it was indicated that the higher accuracy of the image acquisition may make an investigation of musculoskeletal diseases possible.

All MRI scans were performed with a 1.5T body scanner (Siemens Symphony, Erlangen, Germany) in the CHU-Henry Mondor Hospital (Creteil, Paris). The diffusion weighted (DW) images were taken with a b-value of 450 s/mm^{-2} , 12 gradient directions and an effective voxel size of $1.8 \times 1.8 \times 7.8 \text{ mm}^3$ or $1.8 \times 1.8 \times 5.6 \text{ mm}^3$. The repetition time (TR) was 3,600 ms and the echo time (TE) was 104 ms. We investigated a volume of $23 \times 23 \times 15.6 \text{ cm}^3$ and had a acquisition matrix of $128 \times 128 \times 20$ voxels. Moreover, for every subject a T1-weighted with $TR/TE = 465/15$ was taken, that is used for segmentation purposes. Unfortunately, at the beginning we had very strong ghosting artifacts in the DW images, but we were able to get better images with an additional fat suppression activated during the acquisition, see Figure 2.

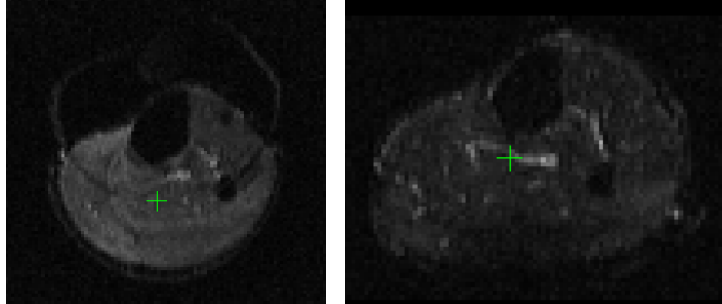


Figure 2: DW image with ghosting (left) and without ghosting (right) as the result of an additional fat suppression.

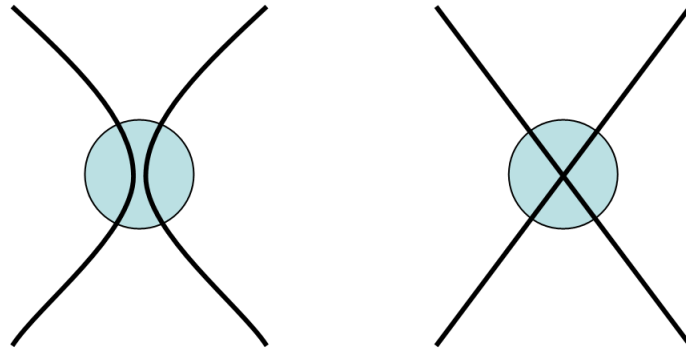


Figure 3: Kissing (left) and crossing (right) fibers lead to problems with the used tensor model because isotropic diffusion is detected although fibers are present.

2.2 Diffusion Measuring

To be able to work with water diffusion from a mathematical point of view, a model has to be found describing it. The most frequently used one was introduced by Basser et al., assuming the presence of anisotropic Gaussian diffusion, that can be described by an ellipsoid [13]. One has to keep in mind that there are cases in which this assumption is no longer valid. For example when two muscle fibers are crossing or kissing in one voxel, then it would be necessary to have two ellipsoids in that voxel to describe it correctly. Using just one ellipsoid leads to a circle that is the result of an averaging that is not correct, see Figure 3. Alternative approaches being more flexible are proposed in [14, 15].

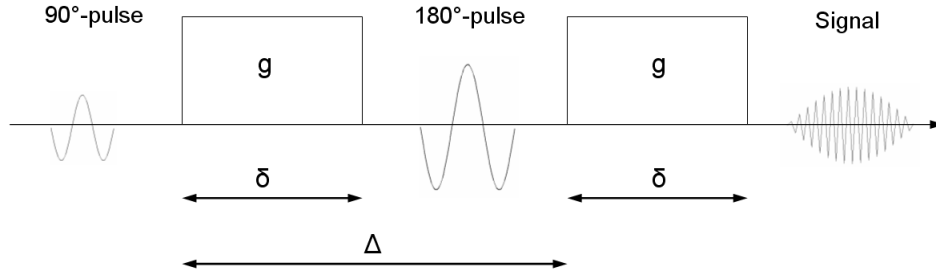


Figure 4: Stejskal-Tanner imaging sequence

The ellipsoids are represented as tensors, which are symmetric positive-definite 3x3 matrices, that have 6 degrees of freedom (DOF). So, for the calculation of the tensors, the diffusion has to be measured for each voxel from at least 6 non-collinear directions. The calculation of the diffusion is done with the Stejskal-Tanner imaging sequence [16]. A diagram with the sequence is shown in Figure 4. The sequence consists of two strong gradient pulses g that are symmetrically positioned around a 180° refocusing pulse, which allows controlled diffusion weighting. Spins that have completed a location change due to the Brownian motion during the time period Δ will get different phase shifts by the two gradient pulses. This results in a signal loss as they are not completely refocused. This signal loss is unwanted for normal T1 and T2 weighted images but it exactly characterizes the diffusion, and making therefore DT imaging possible.

The images still contain anatomical information, although we are only interested in the diffusion, therefore we have to take an image without diffusion weighting S_0 that works as a normalization factor. The diffusion tensor D can then be calculated with the Stejskal-Tanner equation [16]:

$$S = S_0 e^{-bD} \quad (1)$$

with

$$b = \gamma^2 \delta^2 \left(\Delta - \frac{\delta}{3} \right) |g|^2 \quad (2)$$

the diffusion weighting factor defined by LeBihan [17]. The other parameters are the proton gyromagnetic ratio γ , the strength of the diffusion sensitizing gradient pulse $|g|$, the duration of the diffusion gradient pulse δ and the time between diffusion gradient RF pulses Δ , illustrated in Figure 4. The values of D are also known as apparent diffusion coefficients (ADC).

2.3 Calculation of Diffusion Tensors

The more general form of Equation 1 for anisotropic diffusion is

$$S = S_0 e^{-\gamma^2 \delta^2 (\Delta - \frac{\delta}{3}) g^T D g} \quad (3)$$

where g describes the pulse gradient direction and magnitude. This equation can be simplified by setting $\hat{g} = g/|g|$ and using the b-factor of Equation 2

$$S = S_0 e^{-b \hat{g}^T D \hat{g}}. \quad (4)$$

All methods listed below use this equation to get an estimation of the tensor D . The estimation is critical as the acquired images S are quite noisy. Robust estimators and regularizer are proposed to produce better results. A direct estimation of tensors from exactly 7 images is presented in [18]. 7 images are necessary since we need at least 6 diffusion weighted images S_1, \dots, S_6 to have enough equations to calculate the tensor and we also need the normalization image S_0 that is taken without diffusion weighting. The tensor is then calculated with

$$D = \sum_{k=1}^6 \ln \frac{S_0}{S_k} \tilde{g}_k \tilde{g}_k^T. \quad (5)$$

where $\tilde{g}_k \tilde{g}_k^T$ is a specific orthonormal basis. The disadvantage of this approach is its limitation to 7 images which does not enable robust estimation in the presence of noisy images.

The second method is based on a least square estimation [13] of the tensor

$$\min_{D \in M^3} \sum_{k=1}^n \left(\ln \frac{S_0}{S_k} - g_k^T D g_k \right)^2. \quad (6)$$

leading to an over-constrained system. This approach is more robust since it is not limited to 7 images. Two serious drawbacks of these methods were stated by [19]. First, there are no constraints that force the tensor to be positive-definite, and second, the calculation is only point-wise, meaning that no spatial interactions between tensors are considered.

To overcome these drawbacks, Tschumperle proposed a new variational approach that ensures the positivity of the tensor and also a certain regularity [19]. This is described by the following functional:

$$\min_{D \in P(3)} \int_{\Omega} \sum_{k=1}^n \psi \left(\left| \ln \frac{S_0}{S_k} - g_k^T D g_k \right| \right) + \alpha \phi(\|\nabla D\|) d\Omega. \quad (7)$$

where ψ is a function allowing a robust tensor estimation, ϕ is an increasing function acting as an anisotropic regularizer of the tensor field, α is a user-defined regularization weight, $\|\nabla D\|$ is the Frobenius norm and $P(3)$ is the set of symmetric positive-definite matrices. An illustration of the effect of the regularity term can be seen in Figure 5.

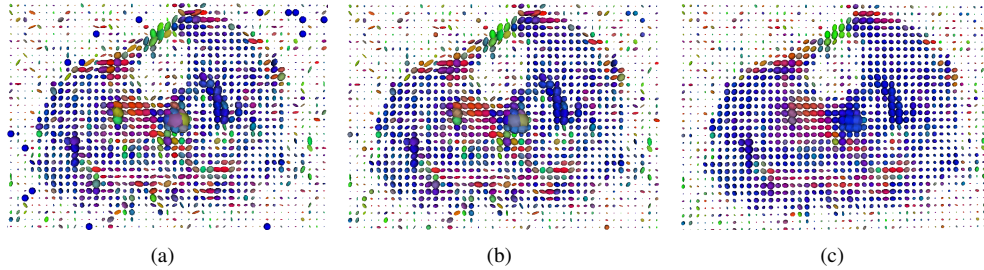


Figure 5: Tensor field with $\alpha = 0$ (a), $\alpha = 0.05$ (b) and $\alpha = 0.5$ (c).

2.4 Interpretation of Diffusion Tensors

In the previous section we presented how to calculate the diffusion tensor, however once calculated, it is not easy to interpret it. Therefore, various coefficients were proposed to illustrate the characteristics of tensors.

2.4.1 Eigenvalues and Eigenvectors

First, a Eigenvalue Decomposition of the tensor can be done so that the three eigenvectors ($\vec{e}_1, \vec{e}_2, \vec{e}_3$) and the three corresponding eigenvalues ($\lambda_1, \lambda_2, \lambda_3$) with $\lambda_1 > \lambda_2 > \lambda_3$ are calculated. As the tensor is positive-definite, a singular value decomposition of the matrix leads to the same result and it is less complex to calculate. The eigenvector \vec{e}_1 , corresponding to the largest eigenvalue points into the direction of the largest diffusion and presents also the principal axis of the ellipsoid.

Tseng et al. showed that there is a correspondence between the primary, secondary, and tertiary eigenvectors to the fiber, sheet, and sheet normal directions, respectively [20]. Galban et al. extended this assumption for the bovine heart, to the skeletal muscle [5]. So that λ_1, λ_2 and λ_3 would represent the diffusive transport along the long axis of a muscle fiber, within the endomysium and the cross-section of a muscle fiber, respectively (see Figure 6). λ_3 would therefore be dependent on the muscle fiber radius. Galban et al. showed also that it is possible to distinguish between functionally different human muscles on the basis of their diffusion properties, especially on the tertiary eigenvector [5]. Unfortunately, these results are not confirmed by [4].

2.4.2 Anisotropy Indices

There is special interest, next to the direction of the diffusion tensor that can be analyzed with the eigenvectors, in the anisotropy of the tensor. The most common indices that are used are the trace of the tensor

$$Tr(D) = \lambda_1 + \lambda_2 + \lambda_3 \quad (8)$$

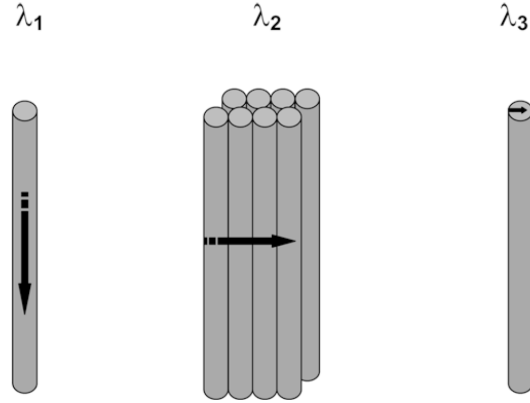


Figure 6: Eigenvectors in muscle [5]

the ellipsoid eccentricity

$$e = \sqrt{1 - \frac{\lambda_3}{\lambda_1}} \quad (9)$$

the fractional anisotropy

$$FA = \sqrt{\frac{3}{2}} \sqrt{\frac{(\lambda_1 - \langle \lambda \rangle)^2 + (\lambda_2 - \langle \lambda \rangle)^2 + (\lambda_3 - \langle \lambda \rangle)^2}{\lambda_1^2 + \lambda_2^2 + \lambda_3^2}} \quad (10)$$

and the relative anisotropy

$$RA = \sqrt{\frac{3}{2}} \sqrt{\frac{(\lambda_1 - \langle \lambda \rangle)^2 + (\lambda_2 - \langle \lambda \rangle)^2 + (\lambda_3 - \langle \lambda \rangle)^2}{(\lambda_1 + \lambda_2 + \lambda_3)^2}} \quad (11)$$

with $\langle \lambda \rangle$ being the average of λ_1 , λ_2 and λ_3 .

3 Pre-processing of images

3.1 Segmentation of muscles

We are concerned with two different types of segmentations: first the segmentation of muscle groups and second the segmentation of healthy and non-healthy tissue. Identifying the different muscle groups is necessary because each muscle has its own characteristics and by calculating parameters over the whole muscle this information gets lost. The reason for the segmentation of the non-healthy

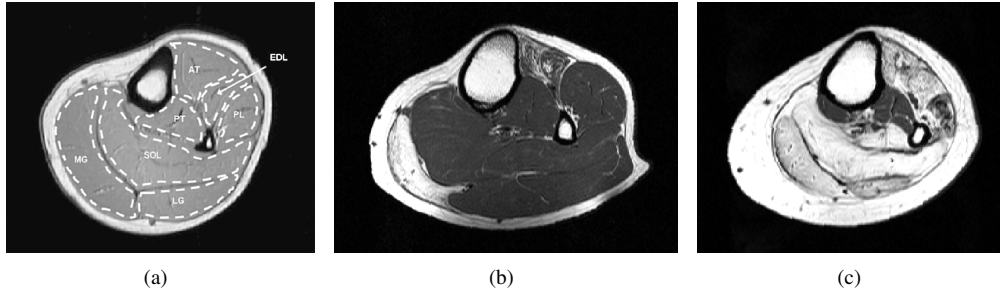


Figure 7: Identified muscle groups (a). The segmentation of non-healthy subjects gets harder the more the disease is spread in the muscle (b) and (c).

tissue is clear since the interest of this study lies in the comparison of healthy and non-healthy tissue. In general, the segmentation can be either proceeded on the T1 images, in the tensor space or in the fiber space. A short description of the three approaches and a proposition of a new semi-automatic segmentation method is given in the following sections.

3.1.1 Segmentation on anatomy images

The segmentation of muscle groups on the anatomy images is done by an expert and serves as ground truth for further segmentation methods. Seven different muscle groups are identified like it was also done by Galban et al. in their study of the human calf [6]. The manual segmentation of muscle groups is time consuming and therefore the need exists to automatize this procedure. The automatic segmentation by using image intensity and image edges in combination with snake segmentation was investigated but it was neither possible to segment muscle groups nor non-healthy structures. The segmentation gets even more complicated for the muscles affected by the myopathy as the boundaries between skin and muscle seem to vanish, see Figure 7.

3.1.2 Segmentation in tensor space

The segmentation in the tensor space uses the diffusion differences between muscle groups to make an automatic segmentation. Since it is supposed that the myopathy changes diffusion properties also the segmentation of non-healthy structure seems possible. The theoretical ability of DTI to differentiate between functionally different muscles was already stated [6]. An additional characteristic of the tensors that can be used is the orientation. Fibers in nonpennate, unipennate and bipennate muscles have different directions so that the direction of the principal eigenvector of tensors should be different. On our data we are not able to automatically differentiate between muscles. The reasons lie in the noisy tensor field and the small absolute differences of the muscles.

3.1.3 Segmentation in fiber space

The segmentation in fiber space uses the fiber tracts (see Section 4). This method was already used for the differentiation of muscle groups in mice [4]. We are investigating this method in more detail in Section 5 but so far it was not possible to make a complete segmentation in different muscle groups. The reason can be seen in the complexity of the task and the low quality of the fiber field. It is not sure if the decrease of spacing in z-direction leads to better results because although the quality of the fibers would get better, the imaged volume would get smaller.

3.1.4 Semi-automatic segmentation method

As shown above, the segmentation of the muscles is a complex task because either it has to be done manually on the anatomy images that takes a lot of time or one of the automatic approaches has to be chosen that do not yet lead to good results. We use a semi-automatic method that bases on the results of [4], who showed that only a small percentage of fibers erroneously jump over into a nearby muscle.

First a manual segmentation of a mid-axial slice in a T1 or T2 volume has to be done. Then the fiber tracts are used to propagate the segmentation to the other slices. So after the propagation, the muscles in the whole volume are segmented. For a schematic illustration see Figure 8. The accuracy of the propagation is very high because of the enormous number of fiber tracts in the volumes.

3.2 Registration

3.2.1 Intra subject

An intra subject registration is necessary as the T1 and DW images are not aligned. The reason for this displacement may be found in the physical acquisition process. The registration is performed with the freely available image registration toolkit (ITK) of Rueckert [21] and normalized mutual information (NMI) as similarity measure. We are applying a rigid registration with 6 DOF (translation and scaling) with good results, see Figure 9.

3.2.2 Inter subject

As stated in Section 3.1, the segmentation of muscles is challenging and up to now only the manual approach produces good results. Therefore, the possibility of having an inter subject registration is very interesting because it would, in combination with an atlas, enable an automatic segmentation. Additionally, the registration parameters transforming one muscle into another could be directly used to analyze the inter-muscle variability.

We were again using the ITK software of Rueckert to perform the registration. A non-rigid registration based on B-splines and NMI was applied but the results were not satisfying. The surfaces

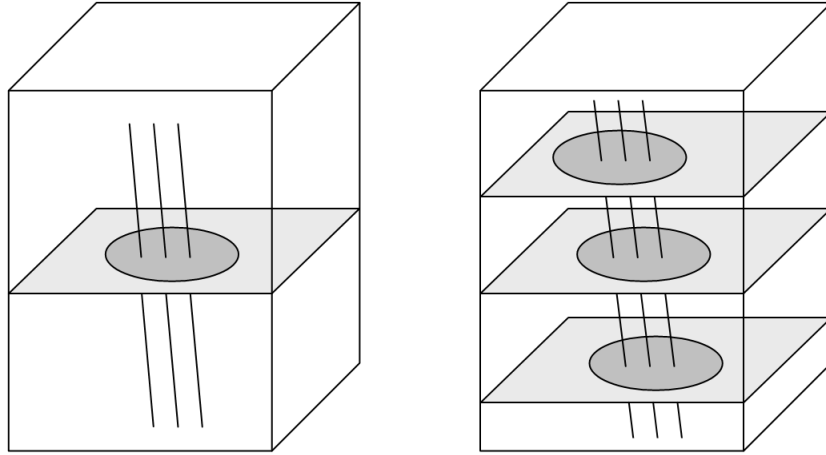


Figure 8: Segmentation of one slice and fiber tracts (left). Propagation of the segmentation with the fiber tracts in the whole volume (right).

of the different legs were matching well, but within the leg it was not possible to match muscle to muscle, see Figure 10. The results were not astonishing having in mind the high variability between the different legs. In contrast to the head, the leg is formed of soft tissue that can even vary from acquisition to acquisition depending on muscle contraction, for example.

So far, the registration was applied to T1 and T2 images. It is, however, also possible to perform the registration between subjects in the tensor or fiber space. Alexander et al. proposed to apply an elastic matching on the diffusion tensor field of human brains [22], whereas Maddah et al. proposed an affine registration between the fiber tracts of human brains [23]. For the human skeletal muscles these approaches seem not feasible because of the high inter-subject variability of the mainly soft tissue in the leg. Also the low quality of the fiber field does not yet allow an acceptable registration between fiber tracts.

4 Fiber Tracking

Fiber tracking also known as tractography tries to reconstruct muscular fibers. There are several reasons that legitimate the application of fiber tracking as being reasonable. First, the muscles are made up of fibers so that there is physical legitimacy. Although one has to be aware of the fact that extracted fibers from the tensor field do not represent real anatomical fibers but coarse-scale properties of fiber bundles. Second, the mass of information in the tensor field and the need for

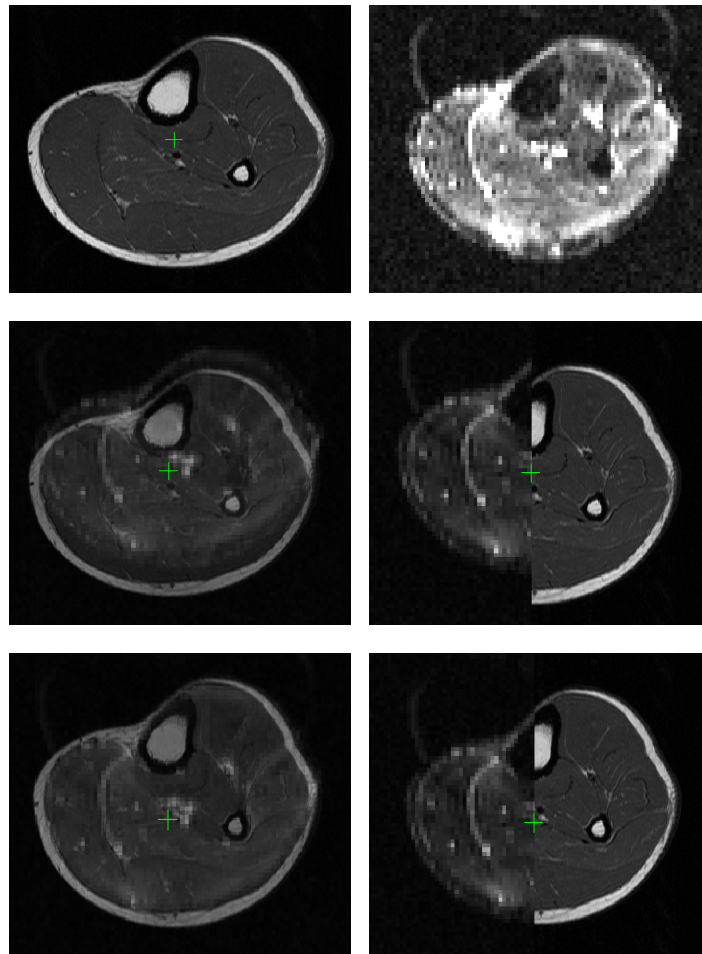


Figure 9: Original T1 and DW images (top row). Superposition of DW and T1 image without registration (middle row). Superposition DW and T1 image with registration (bottom row).

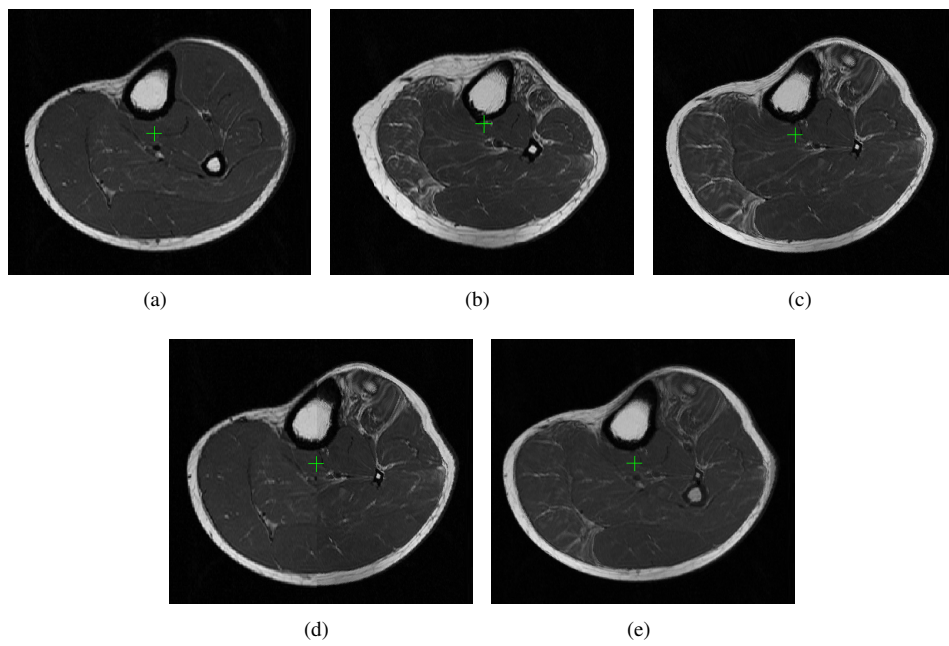


Figure 10: (a) Target and (b) Source of non-rigid registration. (c) transformed source image. Superposition of target and transformed source image (d) and (e).

grouping it in a reasonable way, to make an interpretation possible. The reconstruction of fibers can be seen as a natural and meaningful grouping procedure of tensors.

4.1 Tracking algorithms

Different fiber tracking algorithms were proposed during the past years. Unfortunately, no comparisons between the performances and capabilities have been done. One reason is the lack of a "gold standard" so that there is no possibility to quantify the quality of the tracking. And a second is the complexity of implementing the recent tract-following schemes as they are most times just outlined schematically, making it difficult to reproduce the results and compare the findings [24].

In the literature, three different types of algorithms are proposed to perform the tractography. First, a procedure that follows the direction of the principal eigenvector [25, 26]. Second, a method that integrates over the vector field defined by the principal eigenvector. The numerical integration can be performed by the Euler method, or the 2nd-order and 4th-order Runge-Kutta methods [24]. Third, a stochastic approach that tries to alleviate the shortcomings of deterministic approaches in crossing regions [23].

All approaches have in common that seed points and stopping criteria have to be specified. Seed points are sampled out of the region of interest (ROI) that is defined by the user. It is also possible to automate this process by taking the whole volume as ROI, like it is done in [25]. Stopping criteria limit the fiber tracking to regions where the vector field is robustly specified. In regions with isotropic diffusion, $e_1^{\vec{}}$ has no meaning for the underlying structure, as its direction can be considered random. Typical indices for the restriction are the anisotropy indices (FA, RA), the curviness and the length of the fiber.

4.2 Algorithms in detail

Among others, we used the freely available DTI analysis tool "DTI Track 2005" written by Pierre Fillard to calculate the tractography. It is based on a backward tracking scheme described by Fillard et al. [25] that is an extension of the tracking algorithm proposed by Xu et al. [26]. The principle is to start at the center of the voxel i and follow the principal direction of that voxel $e_{1,i}^{\vec{}}$ until the boundary to a new voxel j is reached. Then the tracking resumes with the direction $e_{1,j}^{\vec{}}$. This continues until one of the stopping criteria is fulfilled. The extension of Fillard et al. was to swap the source and target region, so the tracking is done in the backward direction. During our investigations we used a FA value of 0.18 to stop the tracking.

Another freely available tool that offers fiber tracking is the DTITool described by Vilanova et al. [27]. Heemskerk et al. uses it for the reconstruction of muscle fibers [4]. It is based on the integration of the vector field that is expressed by

$$p(t) = \int_0^t \vec{v}(s) ds \quad (12)$$

with $p(t)$ the fiber and \vec{v} the vector field defined by the principal eigenvector $e_1^{\vec{}}$. The 2nd-order Runge-Kutta method is used as numerical integrator. But also this method like the backward tracking described above has problems with kissing and crossing fibers, see Figure 3. Anatomically, the crossing of fibers in the muscle is quite common because it increases the biomechanical stability. As already stated above, the stochastic approach [23] tries to alleviate these shortcomings. Unfortunately, no accessible implementation is available to test it.

4.3 Tractography results

The fiber tracking algorithm finds about 15,000 to 25,000 fibers per skeletal muscle data set. This is too much to work with. We apply heuristics to prune fibers that have no anatomical significance. This makes a reduction of about 10% possible. Unfortunately, there are still too many fibers remaining so that we use clustering methods to further reduce them, see Section 5.

Generally, it has to be taken into account that fiber tracking performed on a tensor field with an effective voxel size of 8 mm and 6 mm along the z-axis is an ill-posed problem. To get more trustworthy tracts, the effective voxel size has to be further minimized. So far fiber tracking in the muscle has only been applied to DTI images of animals, where the effective voxel size was $0.23 \times 0.23 \times 0.23 \text{ mm}^3$ [4], $0.23 \times 0.23 \times 1.0 \text{ mm}^3$ [3], and $0.55 \times 0.6 \times 0.27 \text{ mm}^3$ [2], which is significantly smaller than our effective voxel size.

5 Fiber Clustering

The motivation to perform clustering on the fiber tracts arises from their enormous number. There is a need to group similar fibers so that the images are easier to interpret and understand. This eases the comparison of characteristics of different fiber bundle types. When looking at Figure 1, one can see that clustering of smaller entities to build larger ones is also practiced in nature. Several myofibrils are bundled together to build the fibers. Several fibers form a fiber bundle and finally, a muscle is made up of several fiber bundles.

A second interest lies in the differentiation between fibers from different muscle groups and fibers from ill and healthy tissue. The problem of the automatic segmentation of muscle groups was already stated in Section 3.1. The differentiation between fibers found in ill and healthy tissue is difficult as we do not expect that the myopathy changes the structure in the muscle. To address this problem we clustered fibers in the diffusivity space and not in the curve space. In the diffusivity space fibers are no more represented by the spatial position of the curve points but by their diffusion characteristics.

Many different fiber clustering algorithms were proposed in the literature but one is confronted with the same problem as for the fiber tracking, the lack of performance evaluation of the algorithms. Therefore it is not possible to rank the algorithms among each other. Mostly a visual inspection of the results by an expert is done. Moberts et al. addressed this problem in his article and proposed

a validation process for fiber clusters [28]. The group of Guido Gerig et al. at UNC Chapel Hill developed FiberViewer, a freely available clustering tool [29] that makes an easy comparison of the proposed methods possible.

The most frequently used distance measures between fiber tracts are:

- Closest point distance
- Mean distance of closest distances
- Hausdorff distance

A precise definition of these distances is given in [30].

It also has to be stated the large part of proposed clustering algorithms are focusing on a clustering of brain fiber tracts. For the muscles, the problem is different so that not all approaches showing good results for the brain are also a good choice for the muscles. Maddah, for instance, proposed an atlas based on clustering with affine registrations between the subjects [23]. As already stated in Section 3.2 the registration between muscles, even by using a non-rigid one, is very complicated.

Couroge et al. is clustering fibers into bundles and analyzing the variability of local shape properties like curvature and torsion within bundles [31]. A Procrustes analysis is performed to align the fibers and to build the mean shape. This makes a characterization of the statistical shape variability possible. This approach was extended by adding diffusion properties to the mean shape [32]. So far, we have neither been able to differentiate between different muscle groups nor between ill and healthy tissue by using the curvature and torsion.

Brun et al. proposed clustering based normalized cuts [33]. First, the fiber traces are mapped to a low-dimensional Euclidean feature space where each fiber is represented by its mean and variance. Then a difference matrix between the fibers is set up by using Gaussian kernels as similarity function. Last, normalized cuts is applied to the difference matrix to get the clustering.

Moberts proposed a framework to validate clustering methods [28]. A manual segmentation serves as ground truth to make a quantitative evaluation and afterwards a verification is done by physicians. Shared nearest neighbor is proposed as a new clustering algorithm.

O'Donnell et al. focused on the determination of correspondences between anatomical clusters across brains [34]. The clustering was done with a spectral approach similar to the k-way normalized cuts procedure. The found cluster-to-cluster correspondence is a key element for the later proposed atlas construction of fiber tracts [35].

Ding et al. proposed a bundling algorithm that considers fibers to be similar if they have comparable length, similar shape, and are separated by a small distance [36]. The bundling algorithm groups together several fibers if their similarity exceeds a certain threshold. As a last step bundle properties like diffusivity, curvature, and torsion are quantified. This clustering approach was used by Damon et al. for the bundling of muscle fibers in rats [37].

Maddah used a statistical mixture model to bundle fibers [38]. Each tract is represented by an equally-spaced sequence of control points from its quintic B-spline representation. An atlas is used as prior information for the clustering, that is performed with an expectation-maximization algorithm.

5.1 K-Means clustering

The k-means is a simple clustering algorithm that we used to reduce the number of fibers. Each fiber is represented by its centroid and then the clustering with about 1,000 classes is launched. Fibers that have the same spatial position are grouped together. Then for each class a representative is chosen which is the fiber that is closest to the center of the class. This leads to a reduction from about 20,000 fibers to 1,000 fibers.

After this reduction of the number of fibers further processing steps like the clustering with FiberViewer were possible. FiberViewer was not able to perform the clustering with more than about 2,000 fibers. It has to be taken into account that this clustering approach is quite simple and does lead to a significant loss of variability within the data set. But it is very fast and the general shape of the fiber field remains.

5.2 Joint probabilistic curve clustering and alignment

A more sophisticated algorithm for clustering fiber tracts is the joint probabilistic curve clustering and alignment algorithm (JCA) presented by Gaffney et al. in [39]. Originally, the method was developed to cluster cyclone curves. The most important feature of this method is the joint clustering and continuous alignment of sets of curves in curve space. This means that the alignment and clustering are not done sequentially, like it is done most times and causes bad results, but at the same time, see Figure 11 for an illustration. Moreover, clustering in curve space means that the curves are not represented as a fixed-dimensional feature vector. The alignment uses model priors and the Expectation-Maximization (EM) learning algorithm. The clustering is done with a finite mixture model.

The curves \mathbf{y}_i consist of a sequence of n_i measurements y_{ij} . The associated covariate of \mathbf{y}_i is the time \mathbf{x}_i , so that x_{ij} gives the time of the measurement y_{ij} . The joint clustering-alignment model is based on a regression mixture model that can be expressed by

$$\mathbf{y}_i = X_i \beta_k + \epsilon_i \quad (13)$$

with ϵ_i is zero-mean Gaussian noise, X_i is the regression matrix, and β_k is the $(p+1) \times 1$ coefficient vector for the k-th cluster. For a polynomial regression, X_i is the standard Vandermonde matrix

$$X_i = \begin{pmatrix} 1 & x_{i1} & x_{i1}^2 & \dots & x_{i1}^p \\ 1 & x_{i2} & x_{i2}^2 & \dots & x_{i2}^p \\ \vdots & \vdots & \vdots & \vdots & \vdots \\ 1 & x_{in_i} & x_{in_i}^2 & \dots & x_{in_i}^p \end{pmatrix} \quad (14)$$

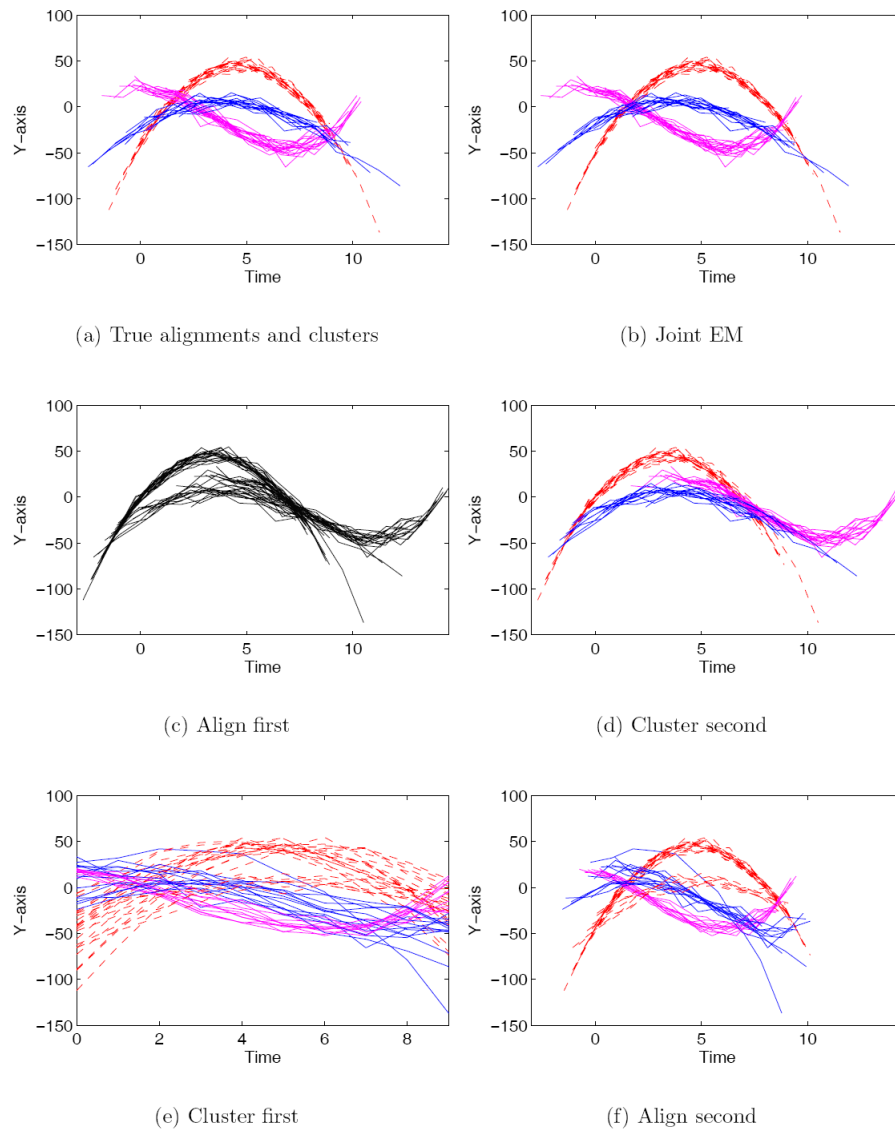


Figure 11: Comparison of joint and sequential clustering: ground truth and result of joint EM (top row), results of first align and then cluster (middle row), results of first cluster and then align (bottom row) [40].

For more flexibility the model is augmented with up to four random transformation parameters $\Phi_i = (a_i, b_i, c_i, d_i)$. The a_i and b_i are for scaling and translation in time, while the c_i and d_i are for scaling and translation in measurement space. The extended model is

$$\mathbf{y}_i = c_i [a_i \mathbf{x}_i - b_i] \beta_k + d_i + \epsilon_i \quad (15)$$

in which $[a_i \mathbf{x}_i - b_i]$ represents the regression matrix X_i at the transformed time $a_i \mathbf{x}_i - b_i$. The probability density of \mathbf{y}_i is expressed by

$$p_k(\mathbf{y}_i | a_i, b_i, c_i, d_i) = \mathcal{N}(\mathbf{y}_i | c_i [a_i \mathbf{x}_i - b_i] \beta_k + d_i, \sigma_k^2 \mathbf{I}) \quad (16)$$

An expectation-maximization (EM) algorithm is derived to estimate the transformation variables Φ_i and the cluster memberships \mathbf{y}_i . The log-likelihood function is defined as the joint log-likelihood of \mathbf{Y} and the hidden data Φ_i, z_i :

$$\mathcal{L}_c = \sum_i \log \alpha_{z_i} p_{z_i}(\mathbf{y}_i | \Phi_i) p_{z_i}(\Phi_i) \quad (17)$$

6 Results of Analysis

In this section the results of our experiments are presented. They are separated into two groups, corresponding to our main interests. First, finding characteristics for different muscle groups, and second, finding characteristics of healthy and non-healthy tissue. For each objective we list the results in the tensor and fiber space, respectively.

6.1 Muscle groups

The interest to find characteristics for different muscle groups is manifold. Being able to quantify well-known anatomical muscle properties like the pennation angle, the fiber length or the PCSA serves as validation for the whole processing chain. This validation is very important, as so far, only visual inspections of the fiber and tensor field were done which allow no evaluation of the accuracy of the reconstruction. Moreover, interest lies in the quantification of the diffusion properties per muscle, hoping that these properties with the anatomical ones would enable an automatic segmentation of muscle groups.

6.1.1 Tensor space

For the differentiation of muscle groups in tensor space, the diffusion coefficients described in Section 2.4 are calculated for muscle groups. The distributions of the FA and Trace values in different muscle groups are shown in Figure 12. No differences between the muscle groups are found because the distributions are identical. Also the use of the third Eigenvalue to differentiate between functional different muscle groups, like proposed by Galban et al., was not possible.

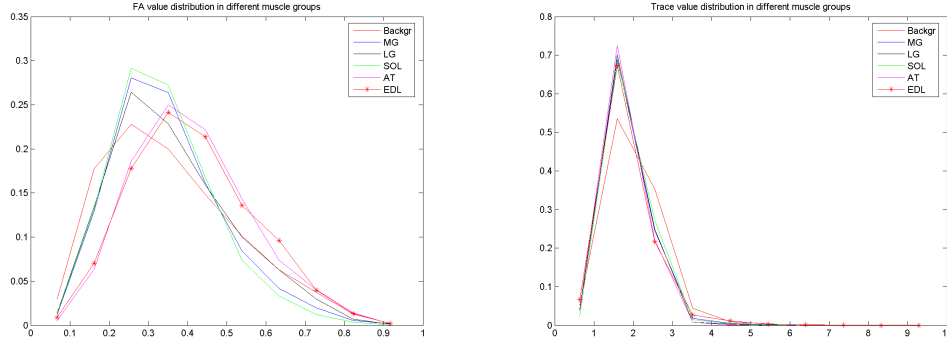


Figure 12: FA and Trace distributions for 5 identified muscle groups. The values are identically distributed in the different muscle groups.

6.1.2 Fiber space

The differentiation of muscle groups in the fiber space is first tried by comparing anatomical properties and then by clustering with the JCA. As already stated in Section 1.1 muscles have a varying pennation angle and fiber length which makes in principal a differentiation possible. The source of the problems that we are confronted with lie in the not satisfying results of the fiber tracts. Uni- and bipennate muscles consist of tendon plates and muscles which should be separated by the tracking algorithm. But in the results that we obtained the fibers are frequently starting with the tendon plate, crossing the muscle by following the fascicles and then continuing with the tendon plate. So tendon plate and fascicles are joined together to one single tract. These tracts make an estimation of the pennation angle not possible and also the analysis of the fiber length is negatively influenced, see Figure 13. Although we are not able to calculate the pennation angle, we are calculating the angle between the main direction of the diffusion ellipsoid and the z-axis, see Figure 13. In the case of tendon plates parallel to the z-axis and a segmentation of the fascicles this makes sense and approximates the real pennation angle. Unfortunately, the segmentation of the fascicles is not possible so that results show a false averaging over tendon plates and fascicles which makes no differentiation between muscle groups possible.

As stated above, the identification of the tendon plate is necessary to measure anatomical muscle properties. We tried to use the JCA to identify the tendon plate in the bipennate soleus muscle. The JCA was applied with all transformation parameters $\Phi_i = (a_i, b_i, c_i, d_i)$, a linear regression model and three classes. In Figure 14 a schematic model of the muscle and the segmentation result is shown. It can be seen that the posterior (green) and anterior (blue) part of the muscle are assigned to different classes. This could be used to identify the tendon plate.

Moreover, we investigate the possibility of using JCA to make an automatic segmentation of the muscle groups. Once again a linear regression model is chosen. The results of the clustering with

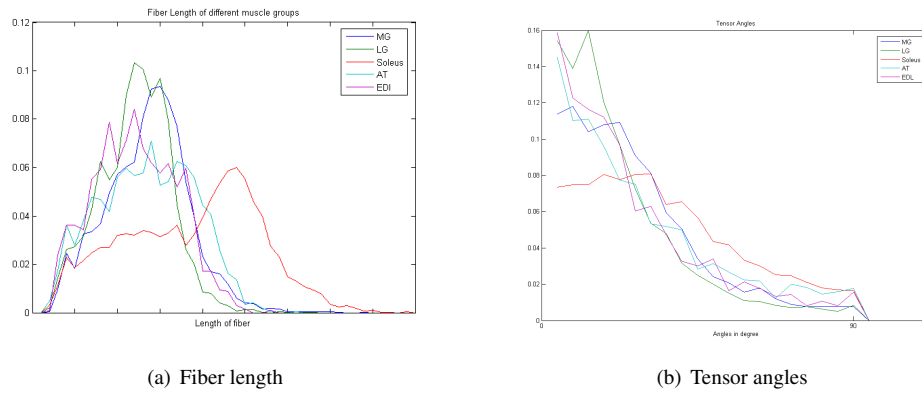


Figure 13: (a) Histogram of fiber lengths for each muscle. Soleus varies from the other muscles with significantly longer fibers which is not the case in the anatomy. (b) Histogram of angles between the principal ellipsoid direction and the z-axis for each muscle.

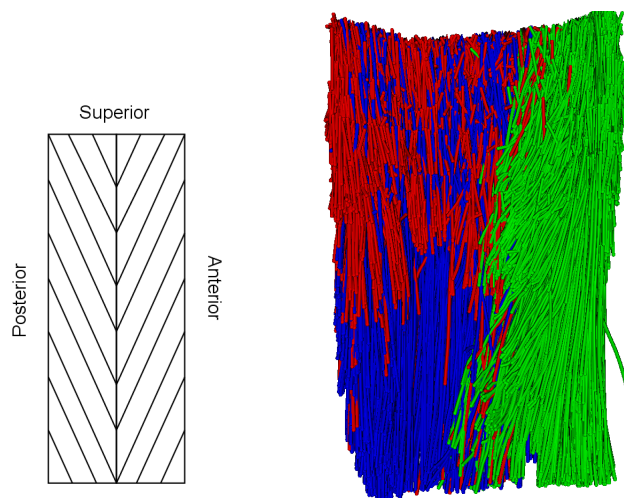


Figure 14: Schematic illustration of the fiber bundles in the anterior soleus (left). Result of joint clustering on the soleus (right).

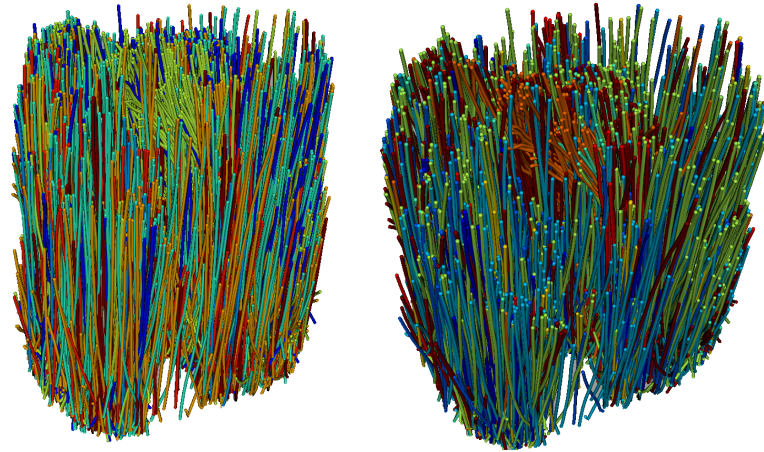


Figure 15: Clustering of muscle with 7 classes (left) and 9 classes (right). Fiber belonging to the same class have the same color.

alignment in curve space with 7 and 9 classes, respectively, are shown in Figure 15. The clustering with alignment in curve and time space does lead to errors during the calculation. It was not possible to differentiate between different muscle groups with this approach. The reasons may lie in the complexity of the task itself and the not satisfying quality of the fiber tracts.

6.2 Healthy and non-healthy muscle

Our second interest is to investigate the effects of the myopathy to the muscle and to find a way to visualize it. We do not expect a change in the architecture or structure of the muscle because the fat cells that replace the muscle cells keep their structure. Instead, the diffusion properties may change. Like in the previous section, first the result of the analysis in tensor space and then in fiber space are presented.

6.2.1 Tensor space

The distribution of the diffusion coefficients on the full image, the foreground, the background, the ill muscles and the healthy muscles is shown in Figure 16. The most interest lies in the comparison of the distributions for ill and healthy muscles. Considering the distribution of the trace of the diffusion tensors no significant difference exists. But when looking at the distribution of the FA coefficient, the distributions for healthy and ill muscles vary. The variance is not so significant that the muscles can be separated by an easy thresholding but it shows that the myopathy influences the diffusion properties.

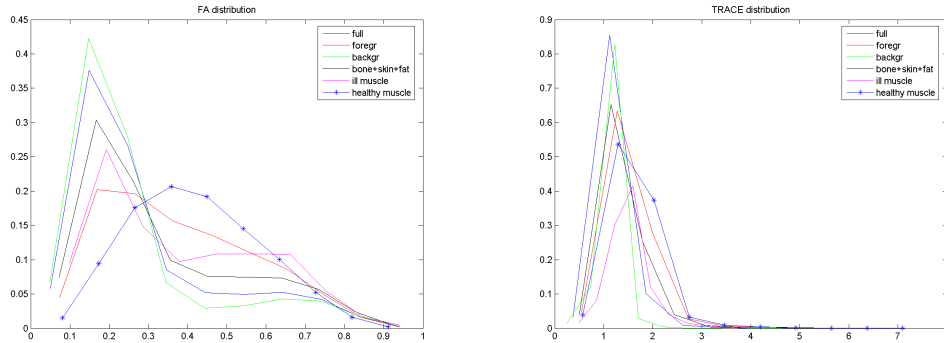


Figure 16: Diffusion distribution of healthy and non-healthy muscle.

6.2.2 Fiber space

First of all it has to be mentioned that the fiber tracking algorithm also found fibers in the non-healthy muscle part. These tracts are similar to them in the healthy muscle part. Therefore we tried to find differences in the diffusion properties along the fiber. FiberViewer has the ability to visualize the diffusion properties along the fiber. A fiber bundle augmented with FA values is shown in Figure 17. Dark colors correspond to low FA values and bright colors to high ones. Normally, the FA values are low at the ends and increase towards the center of the fiber. On non-healthy fiber tracts we also observe low FA values in the middle of the fiber which indicates a change in the diffusion properties along the fiber.

Furthermore, we applied the JCA to the fibers with the augmented FA information. So, the clustering is no longer done in the curve space but in the diffusivity space. The idea is that the clustering algorithm would assign all non-healthy fibers into one class and the healthy ones into another. We applied the JCA with a linear regression model and 2, 3, and 5 classes. A manually segmented volume served as ground truth. The class adjacencies of the real healthy and non-healthy fibers to the class are shown in Figure 18. Like it can be seen, the two types of fibers are in the same classes and no real differentiation is possible.

7 Conclusions

During our study we were encountering several problems. The segmentation of muscle groups was difficult especially for non-healthy subjects as the muscle borders seem to vanish. So we were not able to make a complete analysis and verify our results for several subjects. Also the quality of the fiber tracts is not satisfying which is caused by the low resolution of the acquisitions and the used

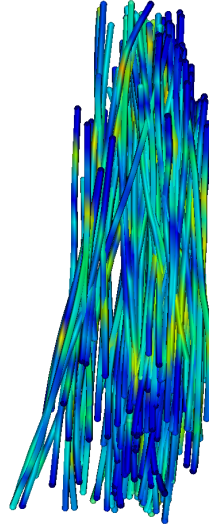


Figure 17: Non-healthy fiber bundle with augmented FA values.

fiber tracking algorithms. The development of a fiber tracking algorithm especially designed for the muscles may be necessary.

But despite these problems we detected changes in the diffusion properties in muscles that are effected by the myopathy. Possibilities to differentiate between ill and healthy fibers were presented but they have not yet lead to good results. A higher resolution of the volumes in the futur will hopefully also lead to better results.

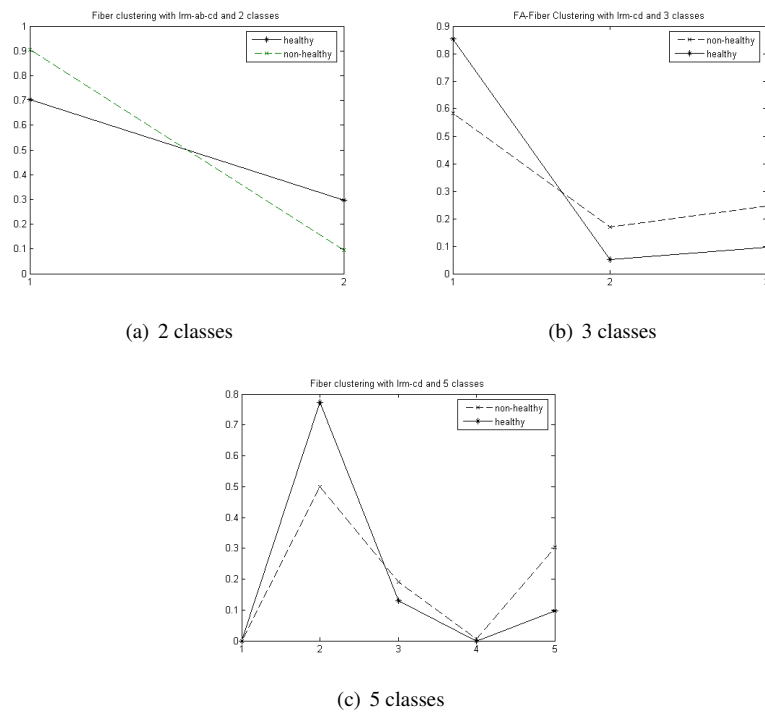


Figure 18: Clustering on the FA value curves of the fibers. The percentage of the healthy and non-healthy in the different classes is shown.

References

- [1] Denis Le Bihan et al., “Diffusion tensor imaging: Concepts and applications”, *Journal of Magnetic Resonance Imaging*, vol. 13, pp. 534–546, 2001.
- [2] C.C. van Donkelaar, L.J.G. Kretzers, P.H.M. Bovendeerd, L.M.A. Lataster, K. Nicolay, J.D. Janssen, and M.R. Drost, “Diffusion tensor imaging in biomechanical studies of skeletal muscle function”, *Journal of anatomy*, vol. 194, pp. 79–88, 1999.
- [3] van Doorn A, Bovendeerd PH, Nicolay K, Drost MR, and Janssen JD, “Determination of muscle fibre orientation using diffusion-weighted mri”, *European journal of morphology*, vol. 34, no. 1, pp. 5 – 10, Feb 1996.
- [4] Heemskerk AM, Strijkers GJ, Vilanova A, Drost MR, and Nicolay K, “Determination of mouse skeletal muscle architecture using three-dimensional diffusion tensor imaging”, *Journal of Magnetic Resonance Imaging*, vol. 53, pp. 1333–40, 2005.
- [5] Craig J. Galban, Stefan Maderwald, Kai Uffmann, Armin de Greiff, and Mark E. Ladd, “Diffusive sensitivity to muscle architecture: a magnetic resonance diffusion tensor imaging study of the human calf”, *European Journal of Applied Physiology*, vol. 93, no. 3, pp. 253 – 262, Dec 2004.
- [6] Galban CJ, Maderwald S, Uffmann K, and Ladd ME, “A diffusion tensor imaging analysis of gender differences in water diffusivity within human skeletal muscle”, *NMR in Biomedicine*, 2005.
- [7] Robert D. Sacks and Roland R. Roy, “Architecture of the hind limb muscles of cats: Functional significance”, *Journal of Morphology*, vol. 173, pp. 185–195, 1982.
- [8] Guus Berenschot, “Visualization of diffusion tensor imaging”, *Master Thesis*, 2003.
- [9] Martha E. Shenton, Ph.D., Marek Kubicki, M.D., Ph.D., Robert W. McCarley, and M.D., “Diffusion tensor imaging image acquisition and processing tools”, *Surgical Planning Laboratory, Technical Report*, vol. 354, 2002.
- [10] Pierpaoli C, Jezzard P, Basser PJ, Barnett A, and Di Chiro G, “Diffusion tensor mr imaging of the human brain”, *Radiology*, vol. 201, no. 3, pp. 637–648, 1996.
- [11] Conturo TE, McKinstry RC, Akbudak E, and Robinson BH, “Encoding of anisotropic diffusion with tetrahedral gradients: a general mathematical diffusion formalism and experimental results”, *Magn Reson Med*, vol. 35, no. 3, pp. 399–412, 1996.
- [12] Usha Sinha and Lawrence Yao, “In vivo diffusion tensor imaging of human calf muscle”, *Journal of Magnetic Resonance Imaging*, vol. 15, no. 1, pp. 87–95, 2002.
- [13] P. J. Basser, J. Mattiello, and D. LeBihan, “Estimation of the effective self-diffusion tensor from the nmr spin echo.”, *J Magn Reson B*, vol. 103, no. 3, pp. 247–254, March 1994.

- [14] Lawrence R. Frank, “Characterization of anisotropy in high angular resolution diffusion-weighted MRI”, *Magnetic Resonance in Medicine*, vol. 47, pp. 1083–1099, 2002.
- [15] David S. Tuch, Timothy G. Reese, Mette R. Wiegell, and Van J. Wedeen, “Diffusion MRI of complex neural architecture”, *Neuron*, vol. 40, pp. 885–895, December 2003.
- [16] E. O. Stejskal and J. E. Tanner, “Spin diffusion measurements: Spin echoes in the presence of a time-dependent field gradient”, *The Journal of Chemical Physics*, vol. 42, no. 1, pp. 288–292, 1965.
- [17] LeBihan D., Breton E., Lallemand D., Grenier P., Cabanis E., and Laval-Jeantet M., “R imaging of intravoxel incoherent motions: Application to diffusion and perfusion in neurologic disorders”, *Radiology*, pp. 401–407, 1986.
- [18] C.-F. Westin, S.E. Maier, H. Mamata, A. Nabavi, F.A. Jolesz, and R. Kikinis, “Processing and visualization for diffusion tensor mri”, *Medical Image Analysis*, vol. 6, pp. 93–108, 2002.
- [19] D. Tschumperlé and R. Deriche, “Variational frameworks for dt-mri estimation, regularization and visualization”, *International Conference on Computer Vision*, 2003.
- [20] Wen-Yih I. Tseng, Van J. Wedeen, Timothy G. Reese, R. Neal Smith, and Elkan F. Halpern, “Diffusion tensor mri of myocardial fibers and sheets: Correspondence with visible cut-face texture”, *Journal of Magnetic Resonance Imaging*, vol. 17, no. 1, pp. 31–42, 2003.
- [21] D. Rueckert, L. Sonoda, C. Hayes, D. Hill, M. Leach, and D. Hawkes, “Nonrigid registration using free-form deformations: Application to breast mr images”, *IEEE Transactions on Medical Imaging*, vol. 8, pp. 712–721, 1999.
- [22] Daniel Alexander, James Gee, and Ruzena Bajcsy, “Elastic matching of diffusion tensor mris”, in *Computer Vision and Image Understanding*, 2000, vol. 7, pp. 233–250.
- [23] Mahnaz Maddah, Andrea U. J. Mewes, Steven Haker, W. Eric L. Grimson, and Simon K. Warfield, “Automated atlas-based clustering of white matter fiber tracts from DTMRI”, in *MICCAI*, 2005.
- [24] Peter J. Basser, Sinisa Pajevic, Carlo Pierpaoli, Jeffrey Duda, and Akram Aldroubi, “In vivo fiber tractography using DT-MRI data”, *Magnetic Resonance in Medicine*, vol. 44, pp. 625–632, 2000.
- [25] P. Fillard, J. Gilmore, W. Lin, J. Piven, and G. Gerig, “Quantitative analysis of white matter fiber properties along geodesic paths”, in *MICCAI’03*, 2003, number 1 in LNCS, pp. 16–23.
- [26] Dongrong Xu, Susumu Mori, Meiyappan Solaiyappan, Peter C. M. van Zijl, and Christos Davatzikos, “A framework for callosal fiber distribution analysis”, *NeuroImage*, vol. 17, pp. 1131–1143, 2002.

- [27] A. Vilanova, G. Berenschot, and C. van Pul, "DTI visualization with streamsurfaces and evenly-spaced volume seeding", in *VisSym '04 Joint Eurographics - I.E.E.E. T.C.V.G. Symposium on Visualization, Conference Proceedings*, 2004, pp. 173–182.
- [28] Bart Moberts, Anna Vilanova, and Jarke J. van Wijk, "Evaluation of fiber clustering methods for diffusion tensor imaging", in *IEEE Visualization*, 2005, pp. 65–72.
- [29] C. Goodlett, I. Corouge, M. Jomier, , and G. Gerig, "A quantitative dti fiber tract analysis suite", *The Insight Journal*, vol. ISC/NAMIC/ MICCAI Workshop on Open-Source Software, 2005.
- [30] Isabelle Corouge, Guido Gerig, and Sylvain Gouttard, "Towards a shape model of white matter fiber bundles using diffusion tensor mri", *ISBI*, pp. 344–347, 2004.
- [31] Isabelle Corouge, Sylvain Gouttard, and Guido Gerig, "A statistical shape model of individual fiber tracts extracted from diffusion tensor mri", *MICCAI*, pp. 671–679, 2004.
- [32] Isabelle Corouge, P. Thomas Fletcher, Sarang C. Joshi, John H. Gilmore, and Guido Gerig, "Fiber tract-oriented statistics for quantitative diffusion tensor mri analysis", *MICCAI*, pp. 131–139, 2005.
- [33] A. Brun, H. Knutsson, H. J. Park, M. E. Shenton, and C.-F. Westin, "Clustering fiber tracts using normalized cuts", in *Seventh International Conference on Medical Image Computing and Computer-Assisted Intervention (MICCAI'04)*, Rennes - Saint Malo, France, September 2004, Lecture Notes in Computer Science, pp. 368–375.
- [34] Lauren ODonnell and Carl-Fredrik Westin, "White matter tract clustering and correspondence in populations", in *MICCAI*, 2005.
- [35] Lauren ODonnell and Carl-Fredrik Westin, "A high-dimensional fiber tract atlas", in *ISMRM*, 2006.
- [36] Zhaohua Ding, John C. Gore, and Adam W. Anderson, "Classification and quantification of neuronal fiber pathways using diffusion tensor MRI", *Magnetic Resonance in Medicine*, vol. 49, pp. 716–721, 2003.
- [37] Damon BM, Ding Z, Anderson AW, Freyer AS, and Gore JC, "Validation of diffusion tensor mri-based muscle fiber tracking", *Magnetic Resonance in Medicine*, vol. 48, pp. 97–104, 2002.
- [38] Mahnaz Maddah, W. Eric L. Grimson, and Simon K. Warfield, "Statistical modeling and em clustering of white matter fiber tracts", in *ISBI*, 2006.
- [39] Scott J. Gaffney and Padhraic Smyth, "Joint probabilistic curve clustering and alignment", in *Advances in Neural Information Processing Systems 17*, Lawrence K. Saul, Yair Weiss, and Léon Bottou, Eds., pp. 473–480. MIT Press, Cambridge, MA, 2005.
- [40] Scott J. Gaffney, "Probabilistic curve-aligned clustering and prediction with mixture models", *Ph.D. Dissertation*, 2004.

Laboratoire MAS – Grande Voie des Vignes – 92290 Chatenay Malabry Cedex

<http://www.mas.ecp.fr>

